Applicability of Ultrasonic Tomographic Technique for Progressive Damage Evaluation in Prismatic Rock Specimen

Butt, Awais
Colorado School of Mines, Golden, Colorado, USA
Fragomeni, Cara
Colorado School of Mines, Golden, Colorado, USA
Hedayat, Ahmadreza
Colorado School of Mines, Golden, Colorado, USA
Tudisco, Erika
Lund University, Lund, Sweden

ABSTRACT: Several damage processes are associated with the loading of intact rock specimens including closure of existing micro-cracks, initiation of cracks, and finally development of cracks. Ultrasonic imaging techniques have proven to be very successful in providing relatively high-resolution images of the damage processes in the rock. Ultrasonic velocity tomography is a full-field measurement technique that can help understand the evolution of damage within a brittle rock specimen remotely and non-destructively. Variations in elastic compressional (P-) wave velocity in a rock specimen can be associated with the changes in its elastic properties under mechanical loading at different stages of damage. The objective of this research study was to examine the applicability of ultrasonic tomographic technique for determination of velocity fields in prismatic rock specimens subjected to uniaxial compression. An array of piezoelectric ultrasonic sensors were used to generate and receive elastic waves across the prismatic specimen and a fast LabVIEW-based data acquisition system was used to record the waveforms. By analyzing and comparing the changes in generated velocity tomograms, through tomographic inversion method, the velocity fields in synthetic and natural rocks were determined.

1. INTRODUCTION

The theoretical strength of brittle materials such as rocks can be higher than their actual strength as much as hundred times, primarily due to the presence of fractures and discontinuities. These naturally occurring features can have a significant influence on the mechanical and hydraulic properties of the rock. Therefore, it is important to understand the several damage processes which are associated with the loading of intact rock specimens including closure of existing micro-cracks, initiation of cracks and their propagation (Hoek and Martin, 2014). Various conventional testing methods used for such evaluation involve performing uniaxial and triaxial testing on the entire specimen without monitoring the localized damage zones. The results from these tests only hold good for perfectly homogenous specimen, but neither material nor the boundary conditions are truly homogenous in any case (Viggiani and Hall, 2008). Full field measurement techniques such as X- ray tomography, Digital Image Correlation, Acoustic emissions, Ultrasonic velocity tomography are among non-destructive techniques that have been used to study the localization of damage in rocks. X-ray tomography provides a full-field measurement for mapping the x-ray attenuation, where attenuation increases with increasing atomic number and density of material (Baruchel et al., 2000). Digital Image Correlation (DIC), which has been used in a wide range of materials (Pan et al., 2009; Dautriat et al., 2010), is a technique used to map the displacement and strain fields on a specimen and is based on finding the displacement between similar regions in a reference and a target image. Acoustic emissions is another full field measurement technique which records the energy released during rock deformation in the form of propagating waves. This method is different from other non-destructive methods such as X-ray tomography and ultrasonic tomography where energy is supplied by an external source. Acoustic emissions technique has been widely used in a variety of rocks (e.g., Zietlow and Labuz, 1998 in Brea sandstone, Lockner, 1993 in granite, Lei et al., 2000 in schist).

Ultrasonic velocity tomography, based on the elastic wave propagation theory, can be used to map the ultrasonic wave velocity for the entire volume of a rock specimen. By determining and comparing the velocity variations (low velocity zones) in the specimen at different stages of damage, it is possible to identify the formation of strain localization zones in the specimen, which are often a precursor to crack initiation, propagation and ultimately material failure. At the laboratory scale, ultrasonic velocity tomography has been used to study the changes in elastic properties due to deformation associated with the loading of a rock specimen (e.g., Hall, 2009). Debski and Young (1999) were able to identify a damaged zone with low velocity zone surrounding the main crack in a cylindrical granite specimen. Mitra and Westman (2009) tried to produce a 3D image of velocity field by combining numerical modelling and 3D ultrasonic tomography on cylindrical samples of Berea sandstone. However, it was not possible to identify the failure plane in the generated velocity tomograms.

In this study, the applicability of ultrasonic velocity tomography technique in identifying the velocity field in natural rocks was evaluated. For this purpose, piezoelectric ultrasonic sensors were used to generate and receive elastic waves across the prismatic Barre granite specimen at multiple locations and a fast LabVIEW-based data acquisition system was used to record the waveforms that provided a great spatial resolution. The resulting velocity tomograms, at different stages of loading, were used to identify the changes occurring in the specimen. The experimental results show a great agreement with the expected velocity ranges for the synthetic (standard) and natural specimens.

2. TOMOGRAPHY

Seismic travel time tomography, which is just an up scaled version of ultrasonic velocity tomography, has been extensively used to image earth's interior structure (Iyer and Hirahara, 1993, Rawlinson et al., 2010). Seismic travel time tomography is a three step procedure: (a) picking of seismic travel times, which is the time taken by the seismic wave to travel from the source to the receiver, (b) estimating the distances travelled, through ray tracing, and (c) constructing travel time equations using inversion to determine the velocities (Padina et al., 2006). Cross-hole transmission tomography is another application area, used for resource exploration and production, which is smaller than the geological application but larger than the current laboratory scale application (Menke, 1984 and Rao and Wang, 2005). Seismic, cross-hole and ultrasonic tomography, all use inverse analysis procedures to determine the wave velocities from calculated travel times (Angioni et al., 2003, Rawlinson et al., 2010, Viggiani et al., 2015).

In elastic wave propagation through a material, the "elastic" term implies that the wave is travelling through the medium without causing any permanent damage or changes. The equation of a wave propagating in an elastic medium is given by (Viggiani and Hall, 2008):

$$\frac{\partial^2 \varepsilon_{vol}}{\partial t^2} = \frac{\lambda+2\mu}{\rho} \nabla^2 \varepsilon_{vol} \quad (1)$$

Ultrasonic waves with small amplitude may not cause any permanent deformation or changes in the medium. Density and elastic properties are the two material properties which can influence the wave propagation in the medium and the changes in these properties can be inferred from the measurements of wave velocity propagating through the medium (Hall, 2009). The velocity is a function of elastic properties as per the elastic theory and the equation for a pure pressure or P-wave is given below:

$$\vartheta_p = \sqrt{\frac{M}{\rho}} \quad (2)$$

In Eq. (1-2), ρ= density, λ and μ are Lame's constants and $M = \lambda + 2\mu$ is the oedometric modulus. From the above equation it can be observed that the wave propagation velocity is inversely proportional to the square-root of density of the material.

3. ULTRASONIC TOMOGRAPHY APPROACH

The first step in applying ultrasonic tomography technique involves recording of the waveforms. It is followed by the process of picking the first arrival time for each waveform. Based on the arrival times, the geometrical parameters (position of all source and receiver positions) are verified and a base velocity model is generated which is required for the final step of inversion. The main steps involved in the ultrasonic tomography are briefly discussed in sections 3.1-3.3.

3.1. Arrival Time Picking

Considering the large number of waveforms typically recorded for tomographic inversion, manual picking of the arrival time is not the most efficient option. Several researchers (Oye et al., 2003; Kurz et al., 2005, Stanchits et al., 2009) have applied different algorithms for automated arrival time picking, which not only avoid time consuming manual picking but also reduce the errors that can be made by the user. In the current study, the automatic arrival time selection has been made through the MATLAB code using Auto regressive - Akaike Information Criterion (AR - AIC) (See Figure 1). This method is based on the work of Morita and Hamaguchi (1984) and assumes that the recorded waveform is a time series with an estimate of the onset time known. The intervals before and after the arrival time of the wave are considered as two different time series and the point where AIC is minimized is the point of separation

between them and thus the arrival time of the wave (Sleeman and Eck, 1999).

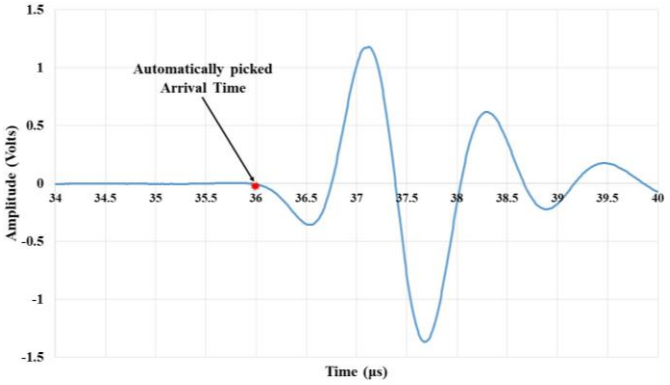

Figure 1. Automatic arrival time picking using AIC algorithm using MATLAB code

3.2. Initial Velocity Model

Before running the inversion algorithm, an initial velocity model is required. In order to obtain this velocity field, all the collected arrival time data are fitted to obtain the unknown geometrical parameters plus the velocity value. In this study, it is assumed that all the geometrical parameters, i.e. the position of source/receiver sensors remain constant between readings. The homogenous velocity field obtained after fitting process is used for the final inversion.

3.3. Inversion

The area of interest in the specimen is discretized into a regular grid of square cells, in each of which the velocity is considered constant. After defining the measured travel time, size of grid cells, ray propagation method and the initial velocity model, the inversion problem is solved by calculating the slowness field. Various methods are available to calculate the over-determined inverse in the inversion process due to number of travel time data being larger than the number of unknowns i.e. the number of cells. Least square method is one of the options; however, in this study two other methods, namely single value decomposition and maximum a posteriori, are used and more information can be found in Charalampidou (2011) and Tudisco (2013).

The result of inversion is a velocity value (or slowness) in each cell with straight ray paths assumed as the ray propagation method. These velocity tomograms obtained at different stages of loading can be compared and analyzed to predict any changes happening inside the specimen.

4. EXPERIMENTAL SETUP

4.1. Sample Preparation

Prismatic specimens of Barre granite, 152.4 mm x 76.2 mm x 25.4 mm were used in this study. Barre granite is an intrusive deposit of Devonian age, obtained from the southwest region of Burlington in Vermont, USA. It is a fine to medium grained rock with mineral grain sizes ranging from 0.25 mm to 3 mm. Feldspar is the main constituent mineral (65% by volume), followed by Quartz (25% by volume) and Biotitic (6% by volume) (Dai and Xia, 2013). The central area of the specimen was selected for ultrasonic imaging as the waves were transmitted without significant attenuation over the 60.325 mm vertical distance. The imaging area measuring 60.325 mm by 76.2 mm is depicted in Figure 2.

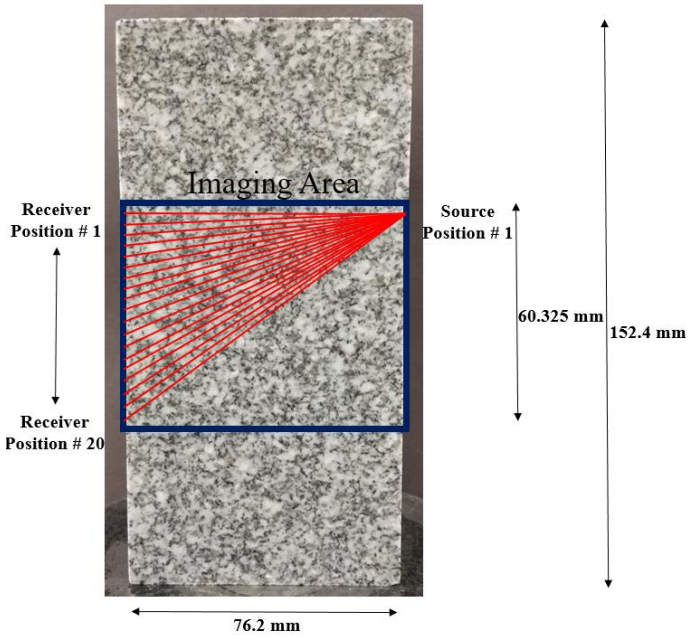

Figure 2. Prismatic Barre Granite specimen indicating the imaging area. Figure also shows the ultrasonic ray paths for Source position # 1 and all 20 receiver positions. Similar pattern for ray paths can be considered for the other 19 source locations and receivers.

4.2. Setup and Data Acquisition System

The complete setup for this study is shown in Figure 3. A pair of contact type video-scan longitudinal (P-) wave piezoelectric sensors were used to generate and receive the waveforms across the prismatic aluminum and Barre granite specimens. The central frequency of the transducer used was 1 MHz and the wavelengths were 6.5 mm and 4 mm for the aluminum and for the Barre granite specimens, respectively. Lab jacks fitted with an in-house built frame to mount the sensor, having a minimum adjust distance of 5μm were used to place the sensors at the exact needed positions shown in Figure 2. The raising or lowering of the lab jacks were maintained precisely by using Linear Variable Differential Transformers (LVDTs) placed on each lab jack. One of the ultrasonic sensor was used as the source and the other as the receiver. During wave acquisitions at each source location, the source sensor was kept stationary and the receiver sensor was moved to the next position. After recording all waveforms emitted from the first source position, the source sensor was moved to the second position and the process was repeated. In this study, the

number of source and receiver positions was twenty on each side of the specimen (Aluminum and Barre granite) and with the interval of 3.175 mm between the consecutive positions.

An Olympus- 5077PR square pulse generator was regulated to produce a 300 volt pulse every 200µs for the source sensor. 100 seismic signals each 100µs long were recorded and stacked to produce a high signal to noise ratio in the transmitted signals. The digitizing rate was 100 Million Samples per second. Fifteen seconds of pause (frequency of 0.06 Hz) was selected between each consecutive wave measurement to ensure ample time for accurate placement of the sensors at the new positions. In order to ensure proper coupling between the specimen and the sensor, oven-baked honey was used. Prior to the experiment, honey was dehydrated in an oven at 100°C for 90 minutes. This procedure was successfully used in previous similar studies (Hedayat et al., 2012; 2014a-d; 2018; Gheibi and Hedayat, 2018a-b). Honey is widely considered as one of the best couplants for P-wave propagation (Couvreur and Thimus, 1996). This complete setup was placed inside the MCC-8 uniaxial loading machine, as shown in Figure 3.

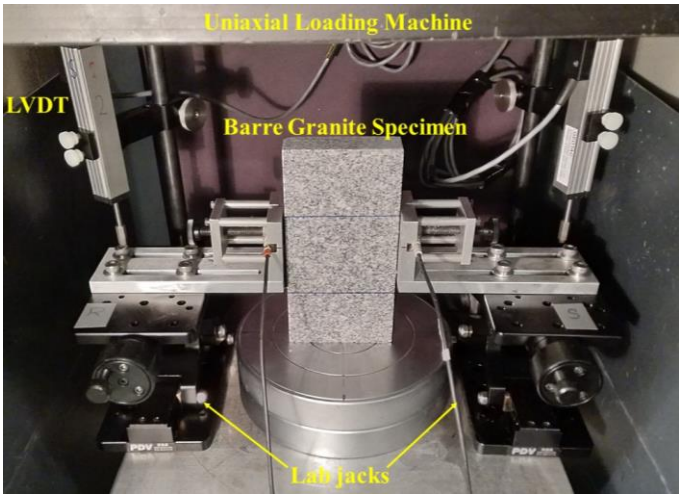

Figure 3. Experimental Setup for ultrasonic tomographic inversion

5. VALIDATION AND APPLICATION

5.1 Validation of the tomographic inversion code

In order to validate the proper functioning of the ultrasonic inversion code written in MATLAB, firstly a synthetic waveform data was generated to be used as input to tomographic inversion. The synthetic waveform data was generated for 32 sources and receivers on each side of the specimen assuming wave transmission without any attenuation. The data generated was for a completely homogenous material with a velocity of 7100 m/s and the arrival time was shifted based on this constant velocity depending on the location of the source and receiver sensors. Figure 4 shows the result of tomographic inversion, confirming that the velocity field is as expected. As a second step of validation, a homogenous prismatic aluminum specimen was used. The waveforms were recorded for 20 source and 20 receiver positions (i.e. 400 waveforms in total). The spacing between each position was 3.175 mm. The results of ultrasonic inversion are shown in Figure 5 in the form of the velocity field.

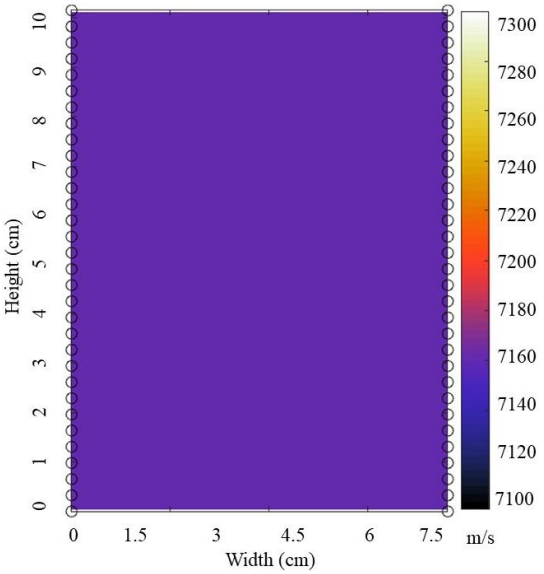

Figure 4. Velocity Tomogram for Synthetic data

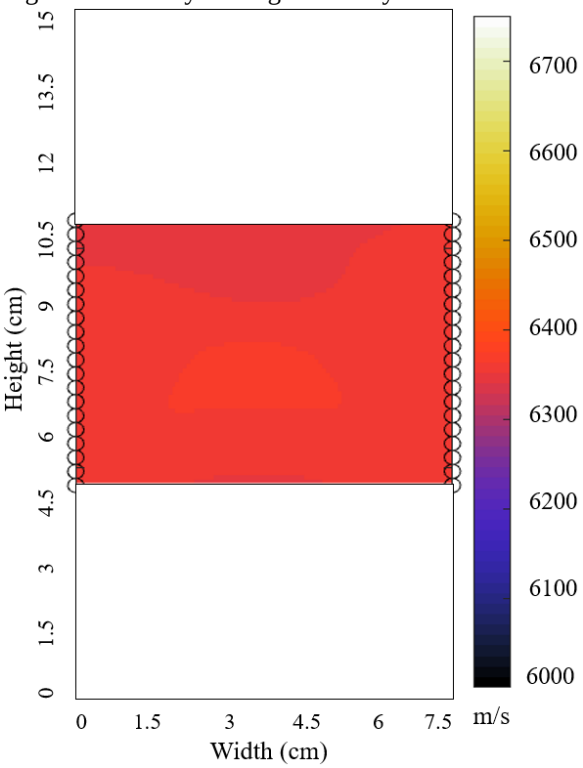

Figure 5. Velocity Tomogram for the Aluminum specimen

The average velocity for this homogenous aluminum specimen as calculated from the tomography work was 6300 m/s and the reported wave velocity for Aluminum material varies between 6200-6400 m/s (Ginzel and Turnbull, 2016). Results shown for both synthetic

waveform data and the aluminum specimen confirm the proper functioning of the tomographic inversion MATLAB code.

5.2 Test on prismatic Barre Granite specimens

After the above verifications, the ultrasonic waveform data was acquired for the area of interest on the prismatic Barre granite specimen and results are shown for the following three stages:

- Before loading the specimen;
- At 80% (142 MPa) of the Unconfined Compressive strength (UCS=175 MPa); and
- After failure of the specimen

Although ultrasonic waveform data was acquired at 20%, 40% and 60% of the unconfined compressive strength as well, the results are not included in this paper as no substantial change was detected, when compared to the unloaded stage. The uniaxial loading test was aborted right before the catastrophic failure of the specimen and after the reduction in the strength (See Figures 6 and 7). The sample retained its original shape although damaged as a result of the uniaxial loading. Velocity tomograms generated for the specimen at the unloaded (intact) stage show a velocity field with a mean velocity of 4170 m/s (See Figure 8). Velocity field for the 80% loading (See Figure 9) shows that the mean velocity for the area imaged in the specimen has reduced to 4028 m/s.

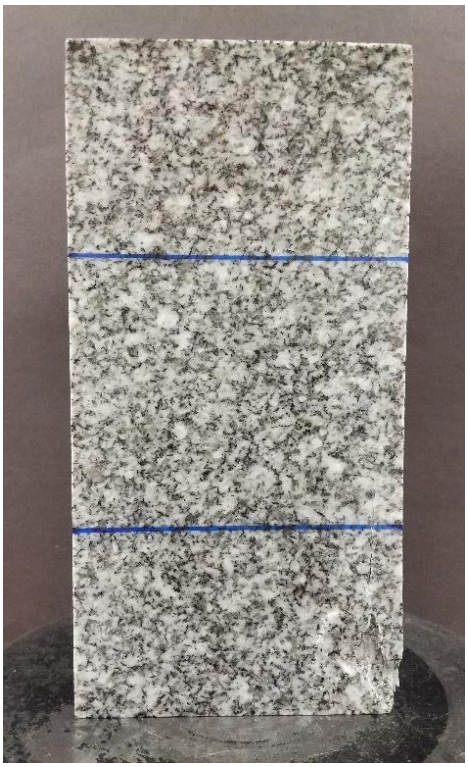

Figure 6. Barre Granite Specimen at failure

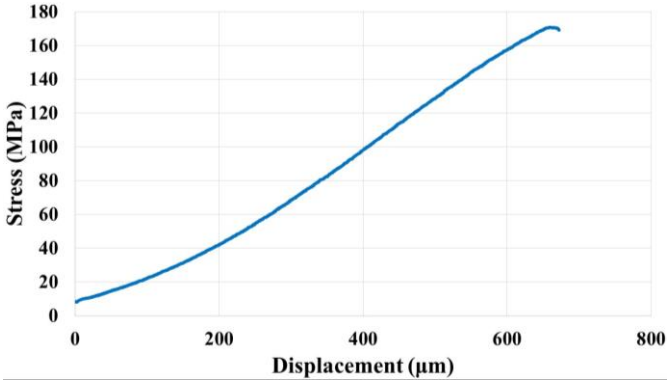

Figure 7. Stress-Displacement for the Barre Granite specimen

Similar results are shown by the velocity tomogram at failure stage (See Figure 10), where the mean velocity is further reduced to 3968 m/s. The band of higher velocity detected in the velocity tomograms for 80% and failure stages (See Figure 9 and 10) are an artefact due to a lower ray density in those regions as indicated in Figure 11. Table 1 presents the maximum and minimum velocity value and standard deviation at different stages for the Barre granite specimen.

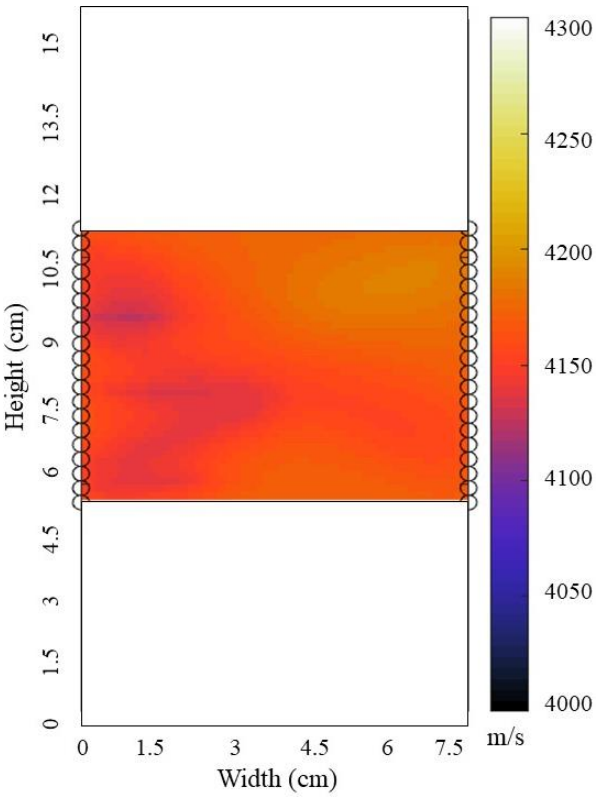

Figure 8. Velocity tomogram for Barre granite specimen at unloaded (intact) stage

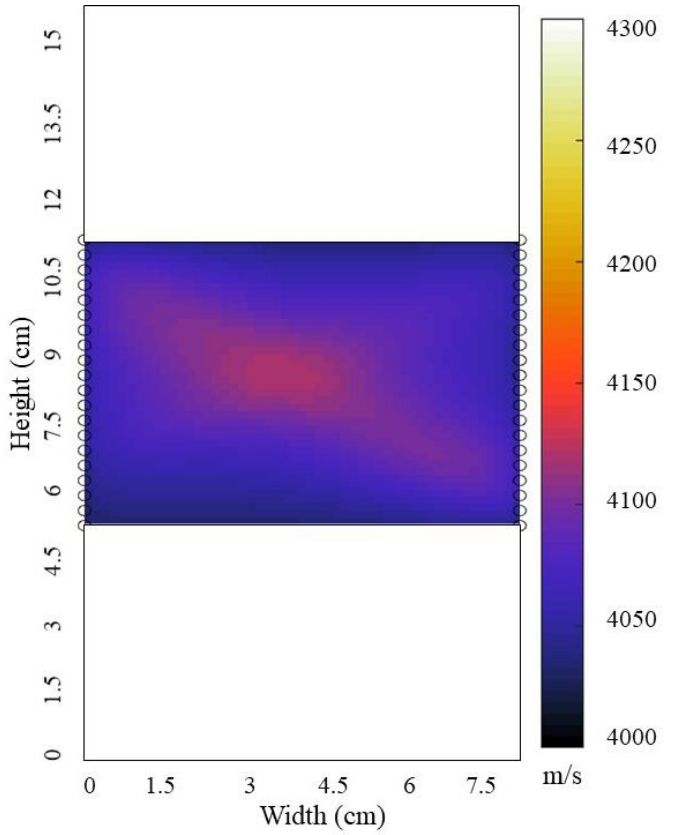

Figure 9. Velocity tomogram for Barre granite specimen after being loaded to 80% of the UCS

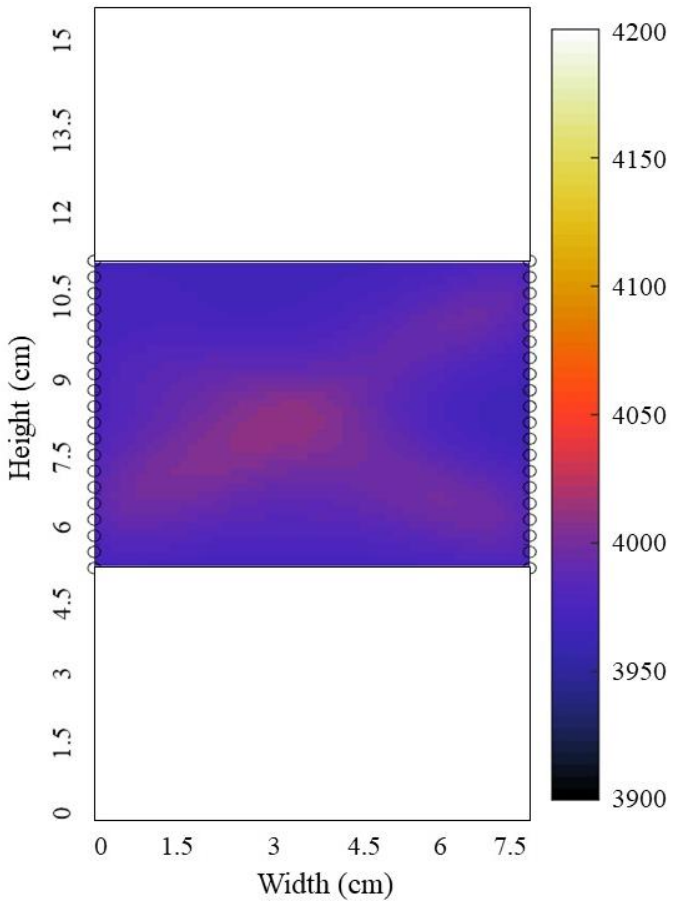

Figure 10. Velocity tomogram for Barre granite specimen just after failure

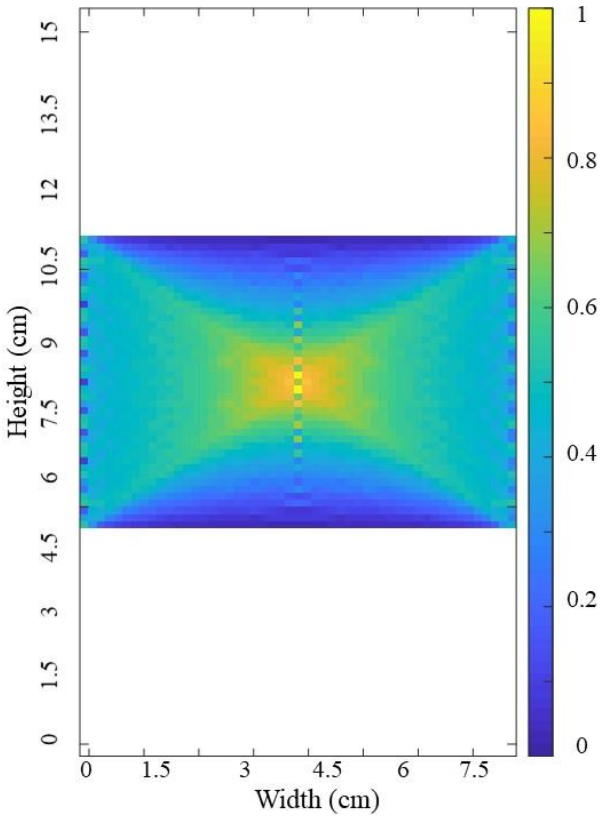

Figure 11. Normalized Ray density with 20 Sources/Receivers for an Imaging area of 60.325 mm by 76.2 mm

Table 1. Velocity data at different stages for Barre granite specimen

Stage	Average Velocity (m/s)	Maximum Velocity (m/s)	Minimum Velocity (m/s)	Standard Deviation (m/s)
Before Loading	4170	4178	4154	4.949
At 80% of the UCS	4032	4041	4027	4.091
At failure	3968	3973	3965	2.093

Upon visual inspection of the failed specimen, no cracking or deformation was observed (See Figure 6). Given the size of the wavelength and the generated microcracks inside the specimen, it is hypothesized that the new cracks did not enlarge enough to be visually detected on the velocity field while the attenuation induced by the addition of cracks was detected by the tomography technique. This suggest that tomographic inversion was able to capture changes in the specimen which were not visible to the naked eye. There is currently an ongoing effort to validate the interpreted velocity field with the strain profile on the surface of the specimen obtained from the DIC analysis.

6. CONCLUSIONS AND FUTURE WORK

This study focused on exploring the applicability of the ultrasonic tomography technique in determination of the velocity field and damage in synthetic and natural rock specimens. It was shown that at different loading stages, the velocity field inside the specimen changes and the mean velocity decreases as the damage extent increases. One limitation of this technique is that when the fractures are significantly smaller than signal wavelength, they remain invisible and when fractures grow and become significantly larger than the wavelengths, they restrict the transmission of ultrasonic waves and attenuate the signals. For such situations, another method like DIC can provide complementary information.

ACKNOWLEDGEMENTS

This material is based upon work supported by the U.S. Department of Energy, Office of Basic Energy Sciences, geosciences program under Award Number DE-SC0019117.

REFERENCES

1. Angioni, T., Rechtien, R. D., Cardimona, S. J., & Luna, R. (2003). Crosshole seismic tomography and borehole logging for engineering site characterization in Sikeston, MO, USA. *Tectonophysics*, *368*(1–4), 119–137. https://doi.org/10.1016/S0040-1951(03)00154-9
2. Baruchel, J., Buffiere, J.Y., Maire, E., Merle, P., Peix, G., 2000. X-ray tomography in material science, Hermes Science Publications, Paris, pp. 1-205.
3. Charalampidou, E., "Experimental study of localized deformation in porous sandstones," Ph.D. thesis, Heriot Watt University and Universite de Grenoble (2011).
4. Dautriat, J., Bornert, M., Gland, N., Dimanov, A., Raphanel, J., 2010. Localised deformation induced by heterogeneities in porous carbonate analysed by multi-scale digital image correlation, Tectonophysics, doi : 10.1016/j.tecto.2010.09.025.
5. Gheibi, A., and A. Hedayat, 2018a. Ultrasonic Investigation of granular materials subjected to compression and crushing. *Ultrasonics Journal*. 87, 112-125.
6. Gheibi, A., and A. Hedayat, 2018b. The Relation between Static Young's Modulus and Dynamic Bulk Modulus of Granular Materials and the Role of Stress History. *Proc. 5th Geotechnical and Earthquake Engineering and Soil Dynamics Conf, GEESDV. Austin. TX. Jun 10-13.*
7. Ginzel, E., & Turnbull, B. (2016). Determining approximate acoustic properties of materials. *NDT.Net*, (July 2016), 1–10. Retrieved from https://www.ndt.net/article/ndtnet/2016/17_Ginzel.pdf
8. Hall, S. A. (2009). Mechanics of Natural Solids. *Mechanics of Natural Solids*, (January 2009). https://doi.org/10.1007/978-3-642-03578-4
9. Hedayat, A., A. Bobet, and L. Pyrak-Nolte. 2012. Monitoring slip initiation and propagation along frictional interfaces with seismic wave transmission. *Proceedings of the 46th US Rock Mechanics Symposium, Chicago, June 24-27.*
10. Hedayat, A., H. Haeri, J. Hinton, H. Masoumi, and G. Spagnoli. 2018. Geophysical signatures of shear induced damage and frictional processes on rock joint. *J. of Geophysical Res*. DOI: 10.1002/2017JB014773.
11. Hedayat, A., L. Pyrak-Nolte. and A. Bobet. 2014a. Precursors to shear failure of rock discontinuities. *Geophysical Research Letters*, 41, 5467-5475.
12. Hedayat, A., L. Pyrak-Nolte. and A. Bobet. 2014b. Detection and quantification of slip along non-uniform frictional discontinuities using digital image correlation. *Geotechnical Testing Journal*, 37 (5).
13. Hedayat, A., Pyrak-Nolte, L and Bobet, A. (2014c). Multi-modal monitoring of slip along frictional discontinuities. Rock Mechanics and Rock Engineering, 47(5), 1575-1587, doi: 10.1007/s00603-014-0588-7.
14. Hedayat, A., L. Pyrak-Nolte. and A. Bobet. 2014d. Geophysical investigation of shear failure along cohesive-frictional rock discontinuities. *Proceedings of the 48th US Rock Mechanics Symposium, Minnesota, June 1-4.*
15. Hoek E, Martin CD (2014) Fracture initiation and propagation in intact rock—a review. J Rock Mech Geotech Eng 6(4):287–300
16. Iyer, H.M. and K. Hirahara. Seismic tomography: theory and practice. Chapman & Hall, 1993. ISBN 9780412371905. http://books.google.it/books?id=km2RV58-9uMcKurz,
17. J. H., Grosse, C. U., & Reinhardt, H. W. (2005). Strategies for reliable automatic onset time picking of acoustic emissions and of ultrasound signals in concrete. *Ultrasonics*, *43*(7), 538–546. https://doi.org/10.1016/j.ultras.2004.12.005
18. Lei, X., Kusunose, K., Rao, M., Nishizawa, O., Satoh, T., 2000. Quasi-static fault growth and cracking in homogeneous brittle rock under triaxial compression using acoustic emission monitoring, J. Geophysical Research, 105, (B3), 6127-6139.
19. Lockner, D., 1993. The role of Acoustic Emission in the Study of Rock Fracture, Int. J. Rock Mech. Min. Sci. & Geomech. Abstr. Vol.30, No.7, pp. 883-899.
20. Menke, W., 1984. The resolving power of cross-borehole tomography. Geophysical Research Letters 11, 105–108.
21. Mitra, R. and E. Westman, "Investigation of the stress imaging in rock samples using numerical modeling and laboratory tomography," in 12th International Conference on Computer Methods and Advances in Geomechanics, Goa (2008), Vol. 2, pp. 1075–1082.
22. Morita, Y., Hamaguchi, H., 1984. Automatic detection of onset time of seismic waves and its confidence interval using the autoregressive model fitting. Zisin 37, 281–293.

23. Oye, V., Roth, M., 2003. Automated seismic event location for hydrocarbon reservoirs, Computers and Geosciences, 29, 851-863.

24. Padina, S., Churchill, D., Bording, R. P. (2006). Travel Time Inversion in Seismic Tomography.

25. Pan, B., Qian, K., Xie, H., Asundi, A., 2009. Two-dimensional digital image correlation for in-plane displacement and strain measurement: a review, Measurement Science and Technology, 20, doi:10.1088/0957-0233/20/6/062001, pp.16.

26. Rao, Y., & Wang, Y. (2005). Crosshole seismic tomography: Working solutions to issues in real data travel time inversion. Journal of Geophysics and Engineering, 2(2), 139–146. https://doi.org/10.1088/1742-2132/2/2/008

27. Rawlinson, N., Pozgay, S., & Fishwick, S. (2010). Seismic tomography: A window into deep Earth. *Physics of the Earth and Planetary Interiors*, *178*(3–4), 101–135. https://doi.org/10.1016/j.pepi.2009.10.002

28. Sleeman, R. and T. van Eck, Robust automatic P-phase picking: an on-line implementation in the analysis of broadband seismogram recordings, Physics of the Earth and Planetary Interiors 113 (1999) 265–275.

29. Tudisco, E., 2009. Ultrasonic and x-ray tomographies to study localised deformation in sandstones, Master Thesis, Université Joseph Fourier, Grenoble, pp. 1-62.

30. Tudisco, E., "Development and application of time-lapse ultrasonic tomography for laboratory characterization of localized deformation in hard soils/soft rocks," Ph.D. thesis, Universite de Grenoble and Universita degli studi di Roma "Tor Vergata," 2013.

31. Viggiani, G. and S. Hall, "Full-field measurements, a new tool for laboratory experimental geomechanics," in Proceedings of the 4th Symposium on Deformation Characteristics of Geomaterials (IOS Press, Amsterdam, 2008), Vol. 1, pp. 3–26.